

Transport of multispecies ion crystals through a junction in an RF Paul trap

William Cody Burton,* Brian Estey, Ian M. Hoffman, Abigail R. Perry, Curtis Volin, and Gabriel Price[†]
Quantinuum, 303 S. Technology Ct., Broomfield, Colorado 80021, USA

(Dated: June 24, 2022)

We report on the first demonstration of transport of a multispecies ion crystal through a junction in an RF Paul trap. The trap is a two-dimensional surface-electrode trap with an X junction and segmented control electrodes to which time-varying voltages are applied to control the shape and position of potential wells above the trap surface. We transport either a single $^{171}\text{Yb}^+$ ion or a crystal composed of a $^{138}\text{Ba}^+$ ion cotrapped with the $^{171}\text{Yb}^+$ ion to any port of the junction. We characterize the motional excitation by performing multiple round-trips through the junction and back to the initial well position without cooling. The final excitation is then measured using sideband asymmetry. For a single $^{171}\text{Yb}^+$ ion, transport with a 4 m/s average speed induces between 0.013 ± 0.001 and 0.014 ± 0.001 quanta of excitation per round trip, depending on the exit port. For a Ba-Yb crystal, transport at the same speed induces between 0.013 ± 0.001 and 0.030 ± 0.002 quanta per round trip of excitation to the axial center of mass mode. Excitation in the axial stretch mode ranges from 0.005 ± 0.001 to 0.021 ± 0.001 quanta per round trip.

Trapped ions are one of the leading candidate systems for scalable quantum computers [1, 2]. In a trapped-ion quantum computer, quantum information is stored in the internal atomic states of the qubit ions, and multi-qubit gates are usually performed by coupling the internal states of two qubits with a common motional mode [3]. Qubit connectivity can be achieved through control of trapping potentials created by surface-electrode ion traps [4–6].

All-to-all connectivity can be achieved either by including all qubits in a single crystal [7] or by use of a quantum charge coupled device (qCCD) architecture [8, 9], where gates are performed on small chains of ions, which can be reordered and reconfigured. Current trapped-ion quantum computers [7, 9, 10] use effectively one-dimensional (linear trap) geometries. In such linear traps, sorting ions between gates is done through a combination of potential well splits [11], rotations [12], and linear transports [11, 13]. Sorting on two dimensional grids additionally requires transport through junctions to connect linear sections. There have been demonstrations of ion transport through several junction geometries, including T junctions [14], wafer-trap [15–17] and surface [18, 19] X junctions, and Y junctions [20–22]. However, there has been no reported effort to transport a multispecies ion crystal through the junction. Doing so allows for simultaneous transport of a sympathetic coolant ion with each qubit, simplifying the sorting algorithm in a large-scale quantum computer.

In this Letter, we present fast, low-excitation junction transport of both single ions and multispecies ion crystals through a microfabricated surface trap X junction fabricated at Honeywell (represented in Figure 1). For single species transport, we used a single $^{171}\text{Yb}^+$ ion, and for multispecies transport, we used a crystal composed of one $^{138}\text{Ba}^+$ ion cotrapped with one $^{171}\text{Yb}^+$ ion (referred to as a Ba-Yb crystal in the remainder of this paper). For both single species and multispecies trans-

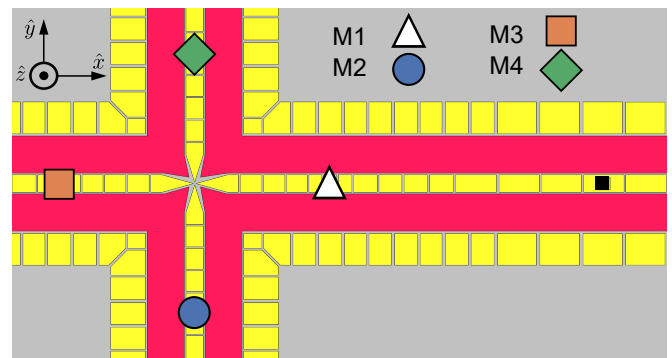


FIG. 1. Cartoon of the junction trap with the junction center at the origin. The RF rails are in red, and the segmented control electrodes are in yellow. There are four measurement zones where we can cool and image the ion: M1 (white triangle) at $(375 \mu\text{m}, 0 \mu\text{m})$, M2 (blue circle) at $(0 \mu\text{m}, -375 \mu\text{m})$, M3 (orange square) at $(-375 \mu\text{m}, 0 \mu\text{m})$, and M4 (green diamond) at $(0 \mu\text{m}, 375 \mu\text{m})$. For experiments in this paper, we initialized the ions in M1 before performing round-trip transports through the junction to the other measurement zones and back.

port, we were able to transport through the X junction to each of the legs (labeled M1-M4 in Figure 1) and back to the starting position with low excitation and without reordering. Additionally, we studied the impacts of transport speed, trap electrode drive voltage drifts, and external stray electric fields to ion excitation and survivability.

Ion surface traps consist of two classes of electrodes: RF rails and segmented control electrodes. When a radio-frequency (RF) oscillating voltage is applied to the RF rails, charged particles in the vicinity undergo micromotion at the RF frequency. This interaction leads to an effective potential $\Phi_{\text{pp}}(\vec{x})$, known as the pseudopotential [1, 23]. For each control electrode, we calculate a basis function $\Phi_i(\vec{x})$ that describes its contribution to the electrical potential at \vec{x} when 1 V is applied to the

TABLE I. Measured axial excitation per round trip of a single ion to the specified end zone and back to M1 at an average speed of 4 m/s. The excitation is measured by sideband asymmetry on the axial mode after a variable number of round trips without cooling, and the slope and statistical uncertainty is reported below.

Crystal	Zone	Round Trip Excitation (quanta)
Yb	M2	0.013 ± 0.001
Yb	M3	0.013 ± 0.001
Yb	M4	0.014 ± 0.001

electrode. The total potential is given by

$$\Phi(\vec{x}) = \Phi_{pp}(\vec{x}) + \sum_i V_i \Phi_i(\vec{x}), \quad (1)$$

where the V_i are the voltages applied to each control electrode. For a given target trapping well (e.g., a potential with a minimum at a defined location and a set of trap frequencies), we can solve for the V_i using a constrained optimization method [17, 24]. To create a waveform of voltages that transports an ion between two locations, we solve for a series of potential wells along the transport path. We then interpolate between these solutions to generate the time-dependent waveform.

The laws of electrostatics place constraints on the sorts of potentials that can be generated. We define the total confinement $C = \nabla^2 \Phi \propto \sum_i \omega_i^2$, where ω_i is the frequency of the i^{th} normal motional mode of harmonic oscillation of a single ion. Because the control electrodes necessarily produce fields with zero divergence, $C \equiv \nabla^2 \Phi_{pp}$ and depends only on the pseudopotential. In other words, no set of control voltages can change the total confinement at a given point – they can only redistribute frequency between modes.

Transport of ions in surface traps have typically followed the path of minimum pseudopotential, which minimizes micromotion and sensitivity to noise on the RF source. In an X junction, the total confinement along the pseudopotential minimum near the center of the junction drops significantly [25]. In this trap, the total confinement at the center of the junction is about 1/8 of its maximum value along the path, as seen in Figure 2b.

A successful strategy in surface-trap junction transport involves moving the ion off of the path of minimum pseudopotential [18, 22]. We define the path of constant total confinement (CTC) as a path directly below (in \hat{z}) the path of minimum pseudopotential, with a height that varies to keep C constant along the path. We choose the value of C so that the path of CTC and the path of minimum pseudopotential intersect above the center of M1. Note that this definition of the path of CTC is independent of ion species. As seen in Figure 2a, the path of CTC drops significantly toward the trap relative to the path of minimum pseudopotential.

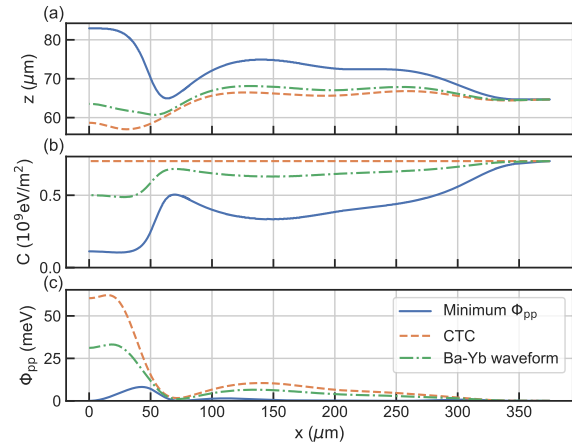


FIG. 2. Properties of the pseudopotential near the junction center along the path of minimum pseudopotential (solid blue line), the path of constant total confinement (CTC) (dashed orange line), and an intermediate path 80% of the way between the two (dot-dashed green line). For a single $^{171}\text{Yb}^+$ ion, we constrain the total potential along the path of CTC, while for a Ba-Yb crystal, we use the intermediate path. The junction center is at $x = 0$ and the center of zone M1 is at $x = 375 \mu\text{m}$. (a) The height of each path above the surface of the trap. Note that the path of minimum pseudopotential and the path of CTC differ by $\sim 20 \mu\text{m}$ at the junction center. (b) The total confinement (C) along each path. Along the path of minimum pseudopotential, C drops significantly, while by construction, it does not vary along the path of CTC. (c) Magnitude of the pseudopotential (Φ_{pp}) for a single $^{171}\text{Yb}^+$ ion along each path. The local maximum at around $x = 25 \mu\text{m}$ is associated with anti-confinement in the axial direction.

For single species junction transport, we generated four waveforms that follow the path of CTC from the junction center to each of the measurement zones (M1, M2, M3, and M4). We define the axial direction to be \hat{x} for M1 and M3, and \hat{y} for M2 and M4 and define the two perpendicular axes to be the radial directions. The total confinement along the path permits waveform solutions that maintain a constant axial trap frequency of 1.13 MHz and a large frequency separation of all motional modes over the entire trajectory, preventing transfer of excitation between the different motional modes [17]. In addition, we created two waveforms that rotate the principal axes of a single well at the center of the junction by 90 degrees, which adiabatically convert the axial direction from \hat{x} to \hat{y} and back. The average speed of the transport can be set by linearly scaling the waveform payout in time.

Each single ion transport experiment begins with a $^{171}\text{Yb}^+$ ion trapped in zone M1. We initialize the system by performing Doppler and sideband cooling [26] to cool all three motional modes to less than 0.1 quanta of excitation each. We then transport the ion to the center of the junction with the time-reversed junction–M1 waveform. To transport to M3, we apply the junction–

M3 waveform. To transport to M2 or M4, we rotate the principal axes while the well center is stationary at the center of the junction before applying the junction–M2 or junction–M4 waveform. We hold the well center position constant for $1 \mu\text{s}$ and then reverse the transport sequence back to M1. The final excitation is measured with Raman sideband asymmetry on the motional mode in the axial direction [26]. To separate non-zero initial temperature from excitation due to transport, we measure the excitation as a function of the number of round-trips and extract the slope, recorded in Table I for transports with average speeds of 4 m/s.

Multispecies crystals present a particular challenge for junction transport because the pseudopotential is proportional to the inverse of the ion mass [23], while the potential due to control electrodes only depends on the ion charge and is thus common to both species. This affects junction transport in two significant ways:

1. At approximately $25 \mu\text{m}$ from the center of the junction, there is a local maximum of the pseudopotential (see Figure 2c), which corresponds to an axial anti-trapping potential. When making a transport waveform for a single ion species, our solution method takes this into account and holds the total axial curvature constant. However for the same waveform, an ion with a different mass will necessarily experience a changing axial curvature, which could lead to excess motional excitation or ion loss.
2. The minimum of the total potential for an ion of one mass occurs at the location where the gradient of the potential from the control electrodes is equal and opposite to the gradient of the pseudopotential. However, the potential minimum for a second ion with a different mass will be at a different position.

Given sufficient degrees of freedom by the control voltages, the total potential for both ion species could be independently controlled. However, this is experimentally impractical since the spacing of an ion crystal is generally of the order of a few micrometers while the distance from the trap and the size of the control electrodes are both about $70 \mu\text{m}$. Instead, we create multispecies junction transport waveforms through a numerical optimization process. We parametrize possible transport waveforms using two degrees of freedom: the path height parameterized by the fraction of the distance between the CTC and the pseudopotential minimum, and the potential curvature in the axial direction. These degrees of freedom have several coupled effects:

1. A larger axial curvature ensures that the total potential for both species remains trapping even at the peak of the anti-curvature of the pseudopotential, but for a given total confinement it reduces the potential curvature in the radial directions.

2. The path height affects both the total confinement and the gradient of the pseudopotential at the ion crystal.
3. The separation of the minima of the total potential for the different ion species is given by a combination of the gradient of the pseudopotential and the curvature in the vertical direction.

Because of the non-trivial coupling, an exhaustive exploration of the parameter space was employed to find successful transport waveforms. At each search point in parameter space, the Ba-Yb waveforms are generated assuming a single synthetic ion with a mass equal to the average ion mass in the Ba-Yb crystal, following the defined transport path, and with a constant total potential curvature in the axial direction. We use a numerical equations-of-motion solver to simulate the behavior of a Ba-Yb crystal during transport in the test waveform and note ion survival and non-adiabatic excitation. We found a broad region of low-excitation waveforms (see Supplemental Material) in parameter space centered around an axial curvature of $9.1 \times 10^7 \text{ eV/m}^2$ (equivalent to a 1.2 MHz axial frequency for the synthetic ion) and a path height 80% of the way between the path of minimum pseudopotential and the path of CTC (dot-dashed green line in Figure 2). We use these parameters for multi-species junction transport for the data collected in the remainder of this paper.

Figure 3 shows the experimental results for multi-species junction transport. We begin each experiment with a Ba-Yb crystal trapped in M1, with the $^{171}\text{Yb}^+$ ion closer to the junction. A combination of EIT cooling on the $^{138}\text{Ba}^+$ and sideband cooling on the $^{171}\text{Yb}^+$ initializes the axial modes with less than 0.05 quanta of excitation, and the radial modes with less than 0.3 quanta of excitation. As in the single species transport experiments, we perform a variable number of round trips between M1 and the other three zones with an average speed of 4 m/s before measuring the excitation in both axial motional modes (center of mass and stretch). The extracted slopes, reported in Table II, indicate that less than or equal to 0.03 quanta of excitation are added per round trip. In addition, we examined the impact of transport speed on induced excitation, with results shown in Figure 3c-d. We find negligible excitation up to 6 m/s. Above this speed, we see evidence of coherent motional excitation in the center of mass (c.m.) mode, which is difficult to quantify with sideband asymmetry measurements. Finally, in the Supplemental Material, we report on the sensitivity of junction transport to drifts in the amplitude of the RF drive and to stray electric fields.

We numerically simulate the properties of a Ba-Yb crystal using the pseudopotential separately scaled by mass for each ion species. In Figure 4a, we plot the simulated equilibrium positions of a Ba-Yb crystal during transport from M1 to the junction center. (The qualita-

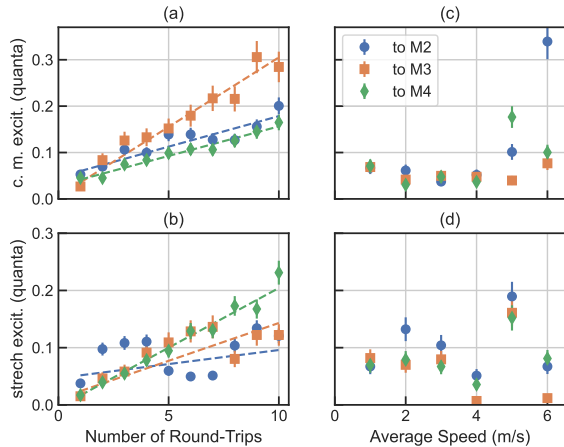


FIG. 3. Measured axial excitation of a Ba-Yb crystal after round trip transports from M1 through the junction to M2 (blue circles), M3 (orange squares), M4 (green diamonds), and back. Error bars are 1σ statistical uncertainty. (a-b) Excitation of the center of mass (c. m.) and stretch motional modes after a variable number of round trips without cooling. The extracted slopes are reported in Table II. (c-d) Excitation of the c. m. and stretch modes after one round trip at a variable speed. The background heating rates of 29 ± 4 quanta/s for the c. m. mode and 3.0 ± 0.5 quanta/s for the stretch mode are not subtracted from the data.

TABLE II. Measured axial excitation per round trip of a Ba-Yb crystal to the specified end zone and back to M1 at an average speed of 4 m/s. The excitation is measured by sideband asymmetry on the specified axial mode after a variable number of round trips without cooling, and the slope and statistical uncertainty is reported below.

Crystal	Mode	Zone	Round Trip Excitation (quanta)
Ba-Yb	c. m.	M2	0.013 ± 0.001
Ba-Yb	c. m.	M3	0.030 ± 0.002
Ba-Yb	c. m.	M4	0.013 ± 0.001
Ba-Yb	stretch	M2	0.005 ± 0.001
Ba-Yb	stretch	M3	0.013 ± 0.001
Ba-Yb	stretch	M4	0.021 ± 0.001

tive features of this waveform are shared by all successful Ba-Yb waveforms found in the numerical optimization.) When the crystal is near M1, where the trapping potential is similar to that generated in a linear surface trap, the crystal is oriented in the axial direction with the $^{171}\text{Yb}^+$ ion closer to the junction. As the crystal approaches the center of the junction, due to different contributions to the total potential from the pseudopotential, it rotates to be perpendicular to the trap (the \hat{z} direction), regardless of the starting leg. When the crystal moves away from the junction center, either reversing its motion or moving into one of the other three legs, the crystal rotates back to a horizontal orientation,

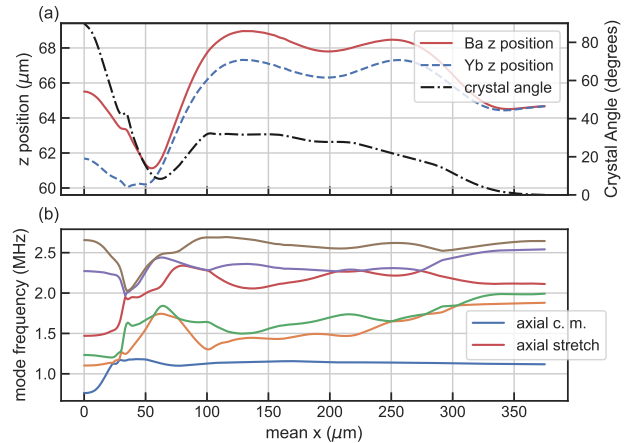


FIG. 4. Predicted properties of the Ba-Yb crystal during junction transport from M1 ($x = 375 \mu\text{m}$) to the junction center ($x = 0$) determined by numerical modeling of the equations of motion. (a) The left axis is the equilibrium height of the $^{138}\text{Ba}^+$ (solid red line) and $^{171}\text{Yb}^+$ ion (dashed blue line) above the trap surface, plotted versus the average x position of the two ions. The right axis is the angle of the crystal rotation (black dot-dashed line). The crystal starts in M1 with the $^{171}\text{Yb}^+$ facing the junction and the $^{138}\text{Ba}^+$ facing away (0 degrees in the xz plane). At the junction center, the crystal is oriented perpendicular to the trap surface (90 degrees). (b) Frequencies of the six normal motional modes of the crystal along the transport path. The axial modes in M1 are labeled. Several mode crossings during transport are predicted.

but always with the $^{171}\text{Yb}^+$ closer to the junction, without an explicit rotation waveform. In Figure 4b, we plot the normal mode frequencies versus ion crystal location. Near $x = 25 \mu\text{m}$, there are several normal mode crossings that couple some of the radial modes to the axial modes during the transport, complicating analysis of transport performed without pre-cooling the radial modes. In experiments where we pre-cool all motional modes, we see no evidence of excitation leaking into the measured axial modes and can conclude that the motional excitation in the radial modes is low.

In this Letter, we have presented the first implementation of junction transport of a multispecies ion crystal, which provides an important tool for minimizing circuit times in a two-dimensional ion trap quantum computer. We find that the transport adds very little excitation to all axial motional degrees of freedom at average speeds up to 6 m/s. In future work, further analysis of the waveform generation method and numerical optimization of the waveform may allow us to control or eliminate the crossing of motional modes during transport or to increase the speed of transport without additional coherent motional excitation [27]. In addition, to demonstrate scalability, we plan to develop the parallel transport of multiple ion crystals through neighboring junctions.

The authors would like to acknowledge Jonathan Andreasen at the Georgia Tech Research Institute for assistance with the surface trap design and Steven Moses at Quantinuum for helpful comments on the text. We thank the entire Quantinuum team for many additional technical and supporting contributions.

* william.burton@quantinuum.com

† gabriel.price@quantinuum.com

- [1] D. J. Wineland, C. Monroe, W. M. Itano, D. Leibfried, B. E. King, and D. M. Meekhof, Experimental issues in coherent quantum-state manipulation of trapped atomic ions, *Journal of research of the National Institute of Standards and Technology* **103**, 259 (1998).
- [2] V. Kaushal, B. Lekitsch, A. Stahl, J. Hilder, D. Pijn, C. Schmiegelow, A. Bermudez, M. Müller, F. Schmidt-Kaler, and U. Poschinger, Shuttling-based trapped-ion quantum information processing, *AVS Quantum Science* **2**, 014101 (2020).
- [3] J. I. Cirac and P. Zoller, Quantum computations with cold trapped ions, *Phys. Rev. Lett.* **74**, 4091 (1995).
- [4] S. Seidelin, J. Chiaverini, R. Reichle, J. J. Bollinger, D. Leibfried, J. Britton, J. H. Wesenberg, R. B. Blakestad, R. J. Epstein, D. B. Hume, W. M. Itano, J. D. Jost, C. Langer, R. Ozeri, N. Shiga, and D. J. Wineland, Microfabricated surface-electrode ion trap for scalable quantum information processing, *Phys. Rev. Lett.* **96**, 253003 (2006).
- [5] D. Leibbrandt, J. Labaziewicz, R. Clark, I. Chuang, R. Epstein, C. Ospelkaus, J. Wesenberg, J. Bollinger, D. Leibfried, D. Wineland, *et al.*, Demonstration of a scalable, multiplexed ion trap for quantum information processing, *Quantum Information & Computation* **9**, 901 (2009).
- [6] S. A. Schulz, U. Poschinger, F. Ziesel, and F. Schmidt-Kaler, Sideband cooling and coherent dynamics in a microchip multi-segmented ion trap, *New Journal of Physics* **10**, 045007 (2008).
- [7] K. Wright, K. M. Beck, S. Debnath, J. Amini, Y. Nam, N. Grzesiak, J.-S. Chen, N. Pisenti, M. Chmielewski, C. Collins, *et al.*, Benchmarking an 11-qubit quantum computer, *Nature communications* **10**, 1 (2019).
- [8] D. Kielpinski, C. Monroe, and D. J. Wineland, Architecture for a large-scale ion-trap quantum computer, *Nature* **417**, 709 (2002).
- [9] J. M. Pino, J. M. Dreiling, C. Figgatt, J. P. Gaebler, S. A. Moses, M. Allman, C. Baldwin, M. Foss-Feig, D. Hayes, K. Mayer, *et al.*, Demonstration of the trapped-ion quantum ccd computer architecture, *Nature* **592**, 209 (2021).
- [10] I. Pogorelov, T. Feldker, C. D. Marciniak, L. Postler, G. Jacob, O. Kriegelsteiner, V. Podlesnic, M. Meth, V. Negnevitsky, M. Stadler, *et al.*, Compact ion-trap quantum computing demonstrator, *PRX Quantum* **2**, 020343 (2021).
- [11] M. Rowe, A. Ben-Kish, B. Demarco, D. Leibfried, V. Meyer, J. Beall, J. Britton, J. Hughes, W. Itano, B. Jelenković, *et al.*, Transport of quantum states and separation of ions in a dual rf ion trap, *Quantum Information and Computation* **2**, 257 (2002).
- [12] F. Splatt, M. Harlander, M. Brownnutt, F. Zähringer, R. Blatt, and W. Hänsel, Deterministic reordering of $^{40}\text{Ca}^+$ ions in a linear segmented paul trap, *New Journal of Physics* **11**, 103008 (2009).
- [13] J. P. Home, D. Hanneke, J. D. Jost, J. M. Amini, D. Leibfried, and D. J. Wineland, Complete methods set for scalable ion trap quantum information processing, *Science* **325**, 1227 (2009).
- [14] W. Hensinger, S. Olmschenk, D. Stick, D. Hucul, M. Yeo, M. Acton, L. Deslauriers, C. Monroe, and J. Rabchuk, T-junction ion trap array for two-dimensional ion shuttling, storage, and manipulation, *Applied Physics Letters* **88**, 034101 (2006).
- [15] R. B. Blakestad, C. Ospelkaus, A. P. VanDevender, J. M. Amini, J. Britton, D. Leibfried, and D. J. Wineland, High-fidelity transport of trapped-ion qubits through an X-junction trap array, *Phys. Rev. Lett.* **102**, 153002 (2009).
- [16] C. Decaroli, R. Matt, R. Oswald, C. J. Axline, M. Ernzer, J. Flannery, S. Ragg, and J. P. Home, Design, fabrication and characterisation of a micro-fabricated stacked-wafer segmented ion trap with two x-junctions., *Quantum Science and Technology* (2021).
- [17] R. B. Blakestad, C. Ospelkaus, A. P. VanDevender, J. H. Wesenberg, M. J. Biercuk, D. Leibfried, and D. J. Wineland, Near-ground-state transport of trapped-ion qubits through a multidimensional array, *Phys. Rev. A* **84**, 032314 (2011).
- [18] K. Wright, J. M. Amini, D. L. Faircloth, C. Volin, S. C. Doret, H. Hayden, C. Pai, D. W. Landgren, D. Denison, T. Killian, *et al.*, Reliable transport through a microfabricated x-junction surface-electrode ion trap, *New Journal of Physics* **15**, 033004 (2013).
- [19] C. Zhang, K. K. Mehta, and J. P. Home, Optimization and implementation of a surface-electrode ion trap junction (2022), arXiv:2201.12579.
- [20] J. M. Amini, H. Uys, J. H. Wesenberg, S. Seidelin, J. Britton, J. J. Bollinger, D. Leibfried, C. Ospelkaus, A. P. VanDevender, and D. J. Wineland, Toward scalable ion traps for quantum information processing, *New Journal of Physics* **12**, 033031 (2010).
- [21] D. L. Moehring, C. Highstrete, D. Stick, K. M. Fortier, R. Haltli, C. Tiggles, and M. G. Blain, Design, fabrication and experimental demonstration of junction surface ion traps, *New Journal of Physics* **13**, 075018 (2011).
- [22] G. Shu, G. Vittorini, A. Buikema, C. Nichols, C. Volin, D. Stick, and K. R. Brown, Heating rates and ion-motion control in a y-junction surface-electrode trap, *Physical Review A* **89**, 062308 (2014).
- [23] J. Drees and W. Paul, Beschleunigung von elektronen in einem plasmabetatron, *Zeitschrift für Physik* **180**, 340 (1964).
- [24] D. Hucul, M. Yeo, S. Olmschenk, C. Monroe, W. Hensinger, and J. Rabchuk, On the transport of atomic ions in linear and multidimensional ion trap arrays, *Quantum Information & Computation* **8**, 501 (2008).
- [25] J. H. Wesenberg, Ideal intersections for radio-frequency trap networks, *Phys. Rev. A* **79**, 013416 (2009).
- [26] C. Monroe, D. M. Meekhof, B. E. King, S. R. Jefferts, W. M. Itano, D. J. Wineland, and P. Gould, Resolved-sideband raman cooling of a bound atom to the 3d zero-point energy, *Phys. Rev. Lett.* **75**, 4011 (1995).
- [27] M. Palmero, R. Bowler, J. P. Gaebler, D. Leibfried, and J. G. Muga, Fast transport of mixed-species ion chains

within a paul trap, Phys. Rev. A **90**, 053408 (2014).

Supplemental material for Transport of multispecies ion crystals through a junction in an RF Paul trap

William Cody Burton,* Brian Estey, Ian M. Hoffman, Abigail R. Perry, Curtis Volin, and Gabriel Price†
Quantinuum, 303 S. Technology Ct., Broomfield, Colorado 80021, USA

(Dated: June 24, 2022)

MULTISPECIES JUNCTION TRANSPORT OPTIMIZATION

In the process of creating transport waveforms for a Ba-Yb crystal, we create test waveforms assuming a single synthetic ion with a mass equal to the average mass in the Ba-Yb crystal. As discussed in the main text, each test waveform is parametrized by the curvature of the total potential in the axial direction and by the ion path, which is given as a weighted combination of the paths of minimum pseudopotential and CTC. In Figure 1, we plot the non-adiabatic excitation predicted by a numerical equations-of-motion solver for a Ba-Yb crystal after applying each test waveform, with results of greater than ten quanta of excitation colored black and less than 10 quanta colored white. The waveform used in the main paper (marked with a red + in the plot) is far from the edges of the region of low excitation.

SENSITIVITY ANALYSIS

Understanding the sensitivity of our waveform generation method to perturbing system drifts helps us estimate the needed recalibration frequency [1]. Therefore, we measured the sensitivity of our transport method to

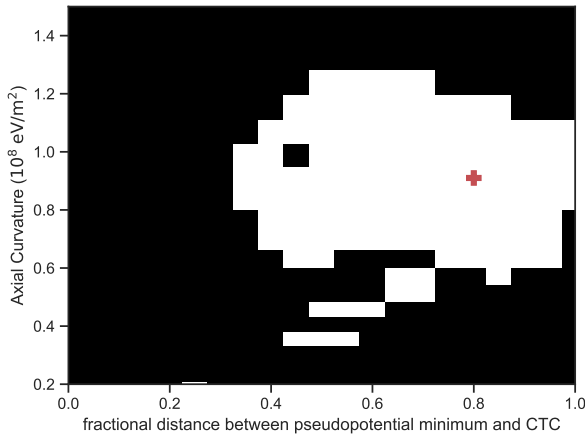


FIG. 1. Plot of results with excitation less than (white) or greater than (black) 10 quanta during numerical optimization. The parameters chosen for this paper are marked with a red +.

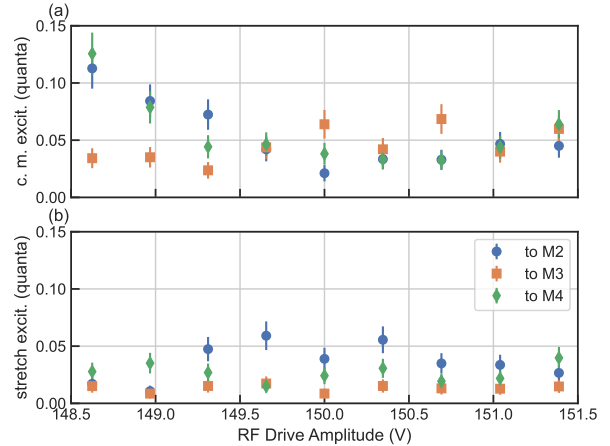


FIG. 2. (a) Center of mass (c.m.) and (b) stretch mode sensitivity to drifts in the RF drive amplitude when Ba-Yb junction transport is performed to zone M2 (blue circles), M3 (orange squares), and M4 (green diamonds).

two major perturbations known to impact ion survivability and transport induced excitation. First, we varied the amplitude of the RF drive for the RF source over a range of $\pm 1\%$ around its nominal value of 150 V, while holding its frequency constant at 44.3 MHz. The resulting axial excitation after one round-trip at an average speed of 4 m/s is plotted in Figure 2. We find that the final excitation is essentially independent of RF voltage at this level.

Additionally, we measured the impact of stray electric fields [2] on our transport method by adding artificial “stray fields” to the transport waveform. At each step of the waveform, we calculated three sets of voltages that give a 1 V/m electric field in \hat{x} , \hat{y} , and \hat{z} , with no curvature, at the equilibrium position of the ion crystal. We scale and add these stray field waveforms to the transport waveform, and then measure the excitation after a round trip as described in the main paper. In Figure 3, we plot the excitation versus applied stray field in each principle direction. For some large applied stray fields, either the crystal becomes untrapped, or the transport induces large coherent oscillation, making sideband asymmetry a poor measure. In those cases, we do not plot any points. The crystal survives with low coherent motion out to ± 400 V/m, ± 600 V/m, and ± 200 V/m for stray fields in the \hat{x} , \hat{y} , and \hat{z} directions respectively. For all directions,

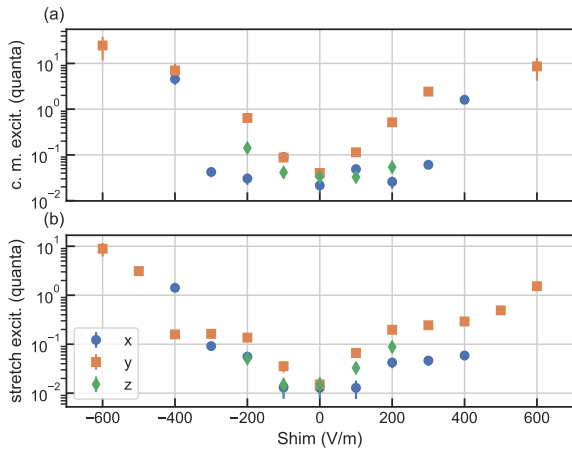


FIG. 3. The sensitivity of the c.m. and stretch mode axial excitation to changes in the bias electric field along the \hat{x} (blue circles), \hat{y} (orange squares), and \hat{z} (green diamonds) directions.

the additional excitation is less than 1 quanta for fields smaller than ± 200 V/m. As a point of reference, typical electrical field drift rates in our system is on the order of ~ 10 V/m over a day, indicating that this waveform generation method is robust against typical drifts.

* william.burton@quantinuum.com

† gabriel.price@quantinuum.com

- [1] J. M. Pino, J. M. Dreiling, C. Figgatt, J. P. Gaebler, S. A. Moses, M. Allman, C. Baldwin, M. Foss-Feig, D. Hayes, K. Mayer, *et al.*, Demonstration of the trapped-ion quantum ccd computer architecture, *Nature* **592**, 209 (2021).
- [2] D. J. Berkeland, J. D. Miller, J. C. Bergquist, W. M. Itano, and D. J. Wineland, Minimization of ion micromotion in a paul trap, *Journal of Applied Physics* **83**, 5025 (1998), <https://doi.org/10.1063/1.367318>.